**ORIGINAL ARTICLE**

# Structural stability of thin-walled austempered ductile iron castings

M. Górny[1]  · Ł. Gondek[2]  · G. Angella[3]  · E. Tyrała[1]  · M. Kawalec[1]  · A. Bitka[4]

**Abstract**

The structural stability of ausferrite in thin-walled Austempered Ductile Iron (ADI) castings with 5 mm wall thickness is compared to a reference casting with 25 mm wall thickness. The thin-walled and reference castings were first austenitized between 850 and 925 °C, and then austempered between 250 and 380 °C. X-ray diffraction (XRD) investigations with changing temperature were performed between − 260 up to + 450 °C to investigate the change of phase fraction, lattice parameters and strain in ausferrite. The role of the austenitization temperature on structural stability and homogeneity of the investigated ADI castings has been provided. In addition, the problem of the occurrence of "blocky" high-carbon austenite that was not completely involved during austempering, has been taken into account. Finally, it has been shown that the thin-walled castings provided higher structural homogeneity and stability if compared to the reference castings.

**Keywords** ADI · Thin-walled casting · Heat treatment · Stability · Homogeneity

## 1 Introduction

Austempered Ductile Irons (ADI) belong to high-quality ductile iron grades with unique properties [1] and wide potential applications, like in automotive [2], military [3], railroad [4] and agricultural industries [5]. Geometrically precise thin-walled castings made of ADIs fit perfectly into the modern trend of interest, thanks to their favorable strength-to-density ratios. Thin-walled ductile iron castings, i.e. castings whose wall thicknesses do not exceed 5 mm, have opened new horizons for high-quality ductile iron to replace steel castings and forgings in many engineering applications with considerable cost benefits [6]. ADIs have the capability to withstand long-term cyclic loads as well as high dynamic impact resistance. In addition, having fatigue resistance higher than aluminum alloys [2], ADIs are predestined for being used in very responsible applications, especially in the form of thin-section components [6].

The process of crystallization and structural formation of thin-walled castings requires tight control because of high cooling rates and very short crystallization times. The casting process that includes the preparation of mold and liquid metal, is characterized by a number of interdependent technological parameters depending on conditions in which the individual technological operations are carried out. Casting geometry, modulus, microstructure, required properties and stability of the production process are the stringent requirements that are necessary for the production of high-tech components.

High-quality ADI castings depend on the casting design, mold quality, proper liquid metal treatment and optimized solid-state refinement process, i.e. heat treatment. The physic-chemical state of the liquid metal and the refining procedure based on spheroidization and inoculation of the liquid metal, determines the microstructure on the casting with a given wall thickness, microstructure that in turn affects the two-step heat treatment to obtain an ausferritic metallic matrix in ADI castings [7]. Bamberger et al. [1] showed that particularly, austenitization mainly affects the homogeneity of the structure, since an increase of austenitization temperature raises the casting austenite fraction,

✉  M. Górny
    mgorny@agh.edu.pl

1   Faculty of Foundry Engineering, Department of Cast Alloys and Composites Engineering, AGH University of Science and Technology, Reymonta St. 23, 30-065 Krakow, Poland

2   Faculty of Physics and Applied Computer Science, Department of Solid State Physics, AGH University of Science and Technology, Mickiewicza Av. 30, 30-059 Krakow, Poland

3   Research Institute CNR-ICMATE, via R. Cozzi 53, 20125 Milan, Italy

4   Łukasiewicz Research Network–Krakow Institute of Technology, Zakopiańska St. 73, 30-418 Kraków, Poland

reducing the number of ferrite plates that result to be thicker and longer. Austempering then affects the morphology of the bainitic ferrite plates, determining the occurrence of upper or lower ausferrite.

In the last four decades a wide body of literature has been produced on the technology and scientific aspects of the structural formation of ADIs. Rouns et al. [8] studied kinetics of austenitizing transformation, Dubensky et al. [9] demonstrated the existence of iron carbides within the ferrite plates, Donini et al. [10] investigated the critical range of austempering times to attain the optimal mechanical properties. The potential for producing thin-walled ADI castings with an ausferritic matrix was presented by Fraś et al. [11] and a qualitative model for ferrite plates formation during the austempering transformation process is shown in the work [12]. The effect of alloying elements and particularly the effect of Nb [13], Cu and Ni [14], Mn [15], nodule count and Ni additions [16] effect on the microstructure and the mechanical properties on ADI were investigated. Bakhshinezhad et al. [17] studied the effects of heat treatment on the mechanical properties of ADI, whereas Haydarzadeh et al. [18] examined tensile behavior of heavy section ADI. Superior wear performance of ADI have been described by Zhang et al. [19], impact toughness by Kim et al. [20] and machinability by Hegde et al. [21]. The effects of austenitizing [22] and austempering kinetics [23] have been widely investigated, also using numerical simulations to predict the dimensional changes [24] and the evolution of phases at the microscale of ADI castings [25]. The stability of ausferrite exposed to a temperature in the range up to 580 °C was studied by Massone et al. [26] while submitted to a non-isothermal annealing up to 700 °C has been described by Perez et al. [27]. Li et al. [28] used neutron diffraction and imaging techniques for multi-scale phase analyses of strain-induced martensite in ADI, whereas Rodriguez-Carvajal [29] studied simulated annealing approach for magnetic structure determination—resulting that ductility and impact strength considerably diminish at high temperature, since ausferrite evolves into a bainite-type structure. Conversely at low temperature, the metastable austenite can transform into martensite, reducing ADI impact strengths. So the ausferrite stability with changing temperatures is an important issue, and stability depends on the microstructure of the original casting before austempering. In thin-walled castings the microstructure is affected by the cooling rate that in turn has significant effect on the microsegregation of alloying elements. This in turn influences the solidification of the primary structure and also the eutectic and eutectoid transformations [1].

To authors' knowledge, no literature is reported on the structural stability of thin-section ADI castings that are annealed at high temperatures or cooled to negative temperatures. The present work also considers the role of different heat-treatment conditions on the homogeneity and thermal stability of a 5-mm thick thin-walled ADI casting. The main objective of this work is, thus, to investigate thin-walled ADI casting behavior with changing temperature from − 260 up to + 450 °C in terms of structural changes through XRD technique, evaluating lattice parameters, phase fraction, lattice strain, and its expansion in the ausferrite microstructure against a reference casting with a typical wall thickness of 25 mm.

## 2 Experimental

The melts were treated in a 15 kg-capacity through using an intermediate frequency induction furnace. The charge was made of Sorelmetal (4.46% C; 0.132% Si; 0.01% Mn; 0.006% S; and 0.02% P), technically pure silica (98% Si), Fe–Mn (76.5% Mn; 6.58% C; 1.35% Si; 0.18% P; 0.018% S), steel scrap (0.2% C; 0.02% Si), copper (99.9% Cu) and nickel (99.99% Ni). The melt was held at 1490 °C for two minute, and then was treated for spheroidization with a 1.3% of Fe-Si-Mg foundry alloy (44–46% Si; 5.5–6.2% Mg; 0.8–1.2% Ca; 0.8–1.2% RE (Rare Earths—contains approximately 50% Ce; 25% La; 15% Nd; 5% Pr; minor amounts of Y and Sm; 0.4–0.8% Al; grain size of 1–10 mm), and then inoculated through bell method with 0.5% of Fe-Si (73—78% Si; 0,75—1,25% Ca; 0,75—1,25% Ba; 0,75—1,25% Al; Fe—residue; grain size 0.5–3.0 mm). The temperature of the spheroidization and inoculation treatments was 1450 °C whereas the holding time before pouring (1400 °C) of liquid metal was 2 min. Thin-walled Y-block iron ingot castings were obtained with 5-mm thickness, whereas a 25 mm thick-wall casting was produced as a reference complying on ASTM A 536–84(2019) e1. Green sand mold, made of silica sand (granularity: 100 to 200 μm), bentonite (7%) and water/bentonite ratio amounted to 0.4. The heat-treatment procedure consisted of austenitization at 850, 875 and 925 °C for two hours in a silite furnace and subsequent austempering at 250, 310, and 380 °C for 4.5, 3 and 1 h, respectively, in a salt bath of $NaNO_2$-$KNO_3$, with final air cooling to room temperature.

SPECTRAMAX emission spectrometer was used for chemical composition determination. The X-ray diffraction (XRD) measurements were performed through using an Empyrean PANalytical powder diffractometer with Bragg–Brentano configuration, Cu Long Fine Focus X-ray tube ($K_\alpha$ line $\lambda = 1.54051$ Å), Ni filter for $K_\beta$ suppression, and curved graphite monochromator. 2θ angles spanned from 20° to 100° with 0.033° step size and an acquisition time of 50 s per step for any temperature measurement. The angular calibration was carried out through using a $LaB_6$ standard. For the low-temperature investigations (15–300 K), an Oxford Instruments PheniX was used, and

any sample position shift because of thermal expansion was corrected with calibrations with high-purity W (99.9999%) powder. High-temperature tests were carried out by means of an Anton Paar HTK 1200 N chamber under high-purity Ar flow (99.9999%) with automatic sample displacement correction. For changing temperature studies, the temperature step was 10 °C with a ramp of 1 °C/min. with a 10 min. stabilization time. Rietveld-type software FullProf was used to refine the collected diffraction patterns [29]. In addition, a Jeol JSM-5500LV Scanning Electron Microscope (SEM) was used for the metallographic study.

# 3 Results and discussion

## 3.1 Microstructure characterization

The casting metallic matrix in the initial state was pearlitic-ferritic, where the ferrite fractions were 8 and 3% in the castings with wall thicknesses 5 and 25 mm, respectively. There were no chills (carbides) presents in the as-cast structure of investigated castings. The quantitative determinations of graphite nodule count $N_F$, mean diameter $d_{eq}$, nodularity $\rho_{nod}$ were $N_F = 485$ mm$^{-2}$, $d_{eq} = 18.2$ μm and $\rho_{nod} = 92\%$ for the thin-walled (5 mm) casting, whilst $N_F = 181$ mm$^{-2}$, $d_{eq} = 27.2$ μm and $\rho_{nod} = 91\%$ were for the reference casting (25 mm). In both cases, the graphite content was $10 \pm 1\%$. So the number of graphite nodules was much higher in the thin-walled casting than in the reference one, which can have significant effects on the diffusion processes during the heat treatments. The number of graphite nodules can be related to the interparticle spacing through a Fullman equation of the following form:

$$\lambda = \frac{1 - f_{gr}}{d_{eq} N_F},\tag{1}$$

where $f_{gr}$ is the volume fraction of the graphite. The interparticle spacing ($\lambda$) can be related to the characteristic diffusional path for the alloying elements, which is also of great importance for the kinetics of the austenitization and austempering processes during the heat treatments. In heavy castings, for instance, where the interparticle distance is usually high [11], the segregation of the alloying elements is difficult to avoid, so this leads to a higher probability of microstructural heterogeneity. It was found that the interparticle spacing was $\lambda = 75$ μm in the thin-walled regions, much smaller than in the reference ones ($\lambda = 155$ μm).

Figure 1 shows selected SEM micrographs of microstructures observed in the thin-walled and reference castings after heat treatments consisting of austenitization at 850, 875 and 925 °C for two hours, subsequent austempering at 250, 310,

and 380 °C for 4.5, 3 and 1 h, respectively, with final air cooling to room temperature.
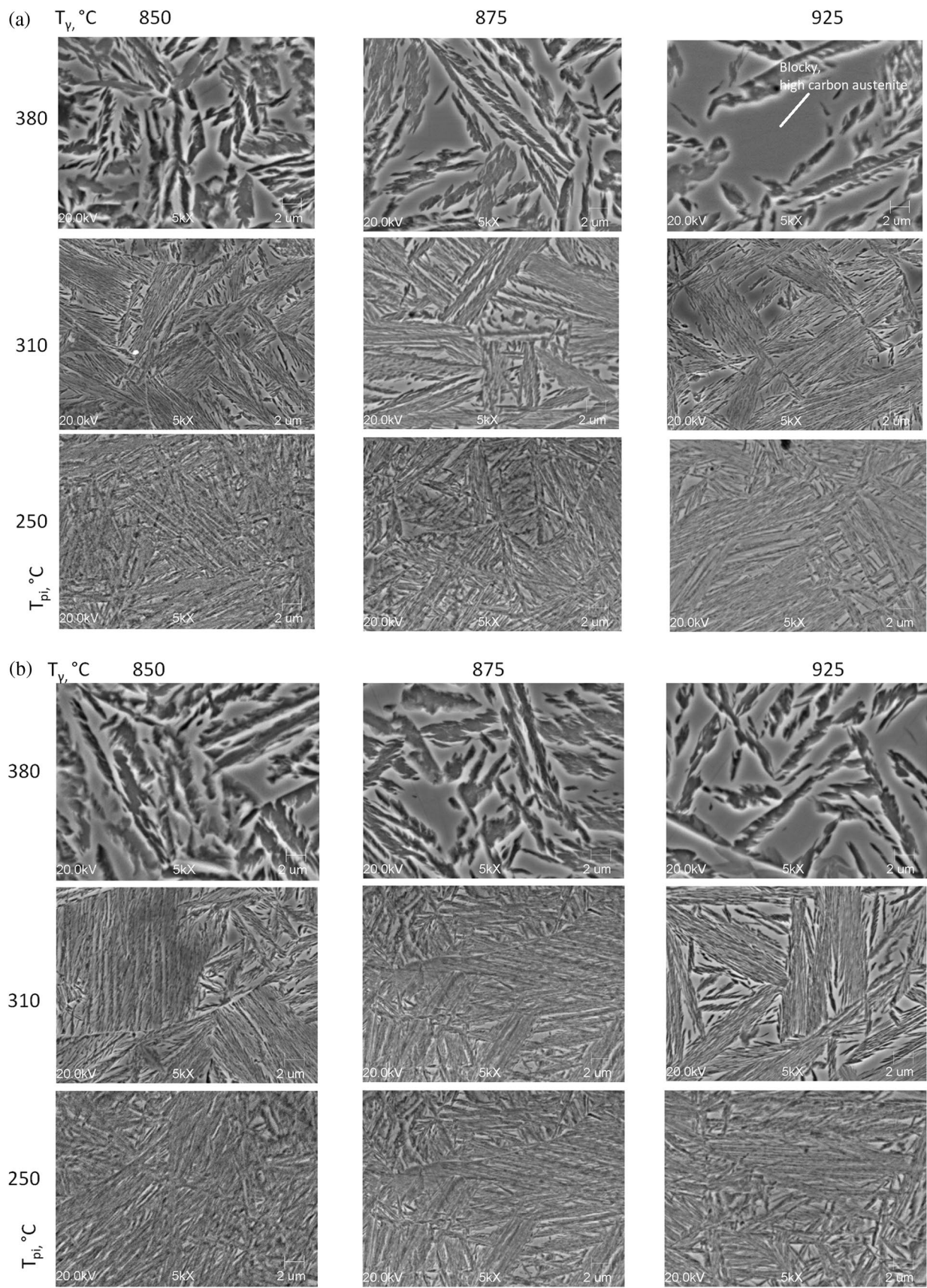
As the austempering and austenitization temperatures decreased, the number of ferrite plates increased, becoming less tattered, and packaged for the lower austempering temperatures, i.e. 310 and 250 °C, which was related to the nucleation and growth rates of bainitic ferrite. Nucleation takes place at the interfacial boundaries of inclusions or austenite grain boundaries due to their high energy, and so a low austempering temperature contributed to the generation of a large number of ferrite nuclei that grow according to the preferred directions. The preferred growth in the [100] crystallographic direction is typical of BCC crystals and reflects the underlying surface energy anisotropy [30]. In the thin-walled castings that had a low interparticle distance, the austenite grain size was much smaller than in castings with a greater wall thickness, resulting in an increase of ferrite platelet packets number. The growth of the ferritic bainite in the preferred direction terminated upon impinging the edge of the another ferrite plate or another ferrite package. Furthermore the degree of the alloying elements segregation is always lower along the preferred growth, and this phenomenon works in favor of thin-section castings from the point of view of their structural homogeneity as well as their thermal stability.

Ausferrite is homogeneous when there is little "blocky" high-carbon austenite that could not be completely involved in ausferrite formation. The local heterogeneity of the ausferrite can give rise to the occurrence of martensite as the result of dynamic loading or, for example, undercooling of the casting component below 0 °C. Indeed blocky austenite could be observed both in the 5-mm walled section and the 25 mm reference castings at any austenitizing temperature, differently to the upper ausferrite produced at 380 °C. From Fig. 1, the ferrite plates number reduced with increasing the austenitizing temperature, whilst their thicknesses enlarged for a given austempering temperature, both in the thin-walled and reference castings. This actually only involved both groups of the investigated castings when heat-treated at the highest austenitizing temperature of 925 °C, and the upmost austempering temperature of 380 °C, respectively.

## 3.2 Chemical composition and XRD analysis

The chemical composition of the investigated ADI is reported in Table 1.

Additions of copper and nickel ensured an ausferritic metallic matrix in the thin-walled castings as well as those with a wall thickness of 25 mm. According to [31], the copper content should not exceed about 0.8–0.9% to avoid the occurrence of highly dispersed $Mg_2Cu$ particles. The correlation between austenitizing and austempering

(a)    $T_\gamma$, °C    850                                   875                                   925



380

310

250

$T_{pi}$, °C

(b)    $T_\gamma$, °C    850                                   875                                   925



380

310

250

$T_{pi}$, °C

◄**Fig. 1** SEM microstructure of thin-walled casting with wall thickness of 5 mm (**a**) and reference casting with 25 mm-thick wall (**b**) vs. austenitization ($T\gamma$) and austempering temperatures ($T_{pi}$)

temperatures with ferrite/austenite volume fractions is shown in Fig. 2 for the thin-walled and reference castings.

In Fig. 2 the high-carbon austenite increased with raising austempering temperature for any austenitizing conditions, whilst the highest ferrite and lowest austenite fractions were obtained at the lowest austenitizing and austempering temperatures (850 and 250 °C, respectively) both for the thin-walled and reference castings. Furthermore, raising the austempering temperature promoted the occurrence of austenite, resulting similar to raising the austenitizing temperature. So the highest austenite fraction was observed in the alloy that was treated at 925/380 °C both for the thin-walled and reference castings. Other than the alloy that was treated at 875/310 °C, the remaining thin-walled castings showed higher ferrite fractions, which originated from the higher ausferritic transformation rate in the thin-wall castings [11]. The highest difference in the ferrite contribution between the thin-walled and reference castings at 12% was achieved at 925 °C, i.e. the highest austenitizing temperature, and the highest austempering temperature of 380 °C. XRD results were consistent with microstructure observations through SEM that are reported in Fig. 1.

The phases lattice parameters determined by XRD are reported in Fig. 3. At first, thinning the wall of the casting led to simultaneous increases both phases lattice parameters. Secondly, the austenite lattice parameters for the thin- and thick-walled castings exhibited maxima for austempering at 310 °C. Thinning the casting walls generally led to rising austenite and ferrite lattice parameters for the same thermal treatment. For the lowest austenitizing temperature (850 °C), the above-mentioned change was within uncertainty levels, both for the austempering temperatures of 250 and 380 °C.

It has been established that the austenite lattice parameter is linearly proportional to the carbon content according to empirical formula [32]:

$$a_\gamma = 3.555 + 0.045 \cdot C_\gamma - 0.0019 \cdot Si_\gamma [AA], \quad (2)$$

where $a_\gamma$ is the austenite lattice parameter (Å), and $C_\gamma$ and $Si_\gamma$ are the carbon and silicon contents in the austenite (wt.%), respectively. In accordance with Eq. 2, the austenite lattice parameters depend on the final carbon content in austenite, which determines the stability of the structure. At a carbon content lower than 1.8 wt.%. [1] austenite can partially transform into martensite as a result of dynamic loading or, for example, undercooling to negative temperatures. This phenomenon is quite undesirable, as it significantly reduces the dynamic properties for ADI castings with upper ausferrite.

The changes in the above lattice parameters can be associated with the ausferrite formation, as during austempering solid-state transformation, only a small fraction of the carbon goes into ferrite, whilst the rest stays in austenite that can have in solution up to about 2 wt.% of C. Furthermore the formation of unfavorable blocky austenite can be indirectly seen in Fig. 3, being the cause of the decrease of austenite lattice parameter for the high austenitizing and austempering temperatures (925/380 °C).

The rise of the thin-walled ferrite lattice parameters with regard to the reference casting should be attributed to the faster kinetics of the austempering process due to the greater number of graphite nodules and smaller interfacial distances. In both the thin-walled and reference castings, the lowest austenitizing temperature resulted in a local maximum of the ferrite lattice parameter for austempering at 310 °C. This should be counterbalanced by a much greater fraction of austenite in ausferrite, suggesting that accelerated diffusive carbon transport occurred appreciably. For the thin-section castings, higher values of ferrite lattice parameters were obtained for the applied austenitizing temperatures of 875 and 925 °C as compared to the reference castings, even austempering at 250 °C. So austenitizing temperature affected significantly ferrite plates nucleation and growth which had a higher degree of carbon saturation in the thin-section castings than in the reference castings. This may also indicate greater structural stability. The low austenite fraction at low austempering temperatures, and the subsequent slow diffusion processes made difficult for carbon diffuse from the bainitic ferrite to austenite, resulting in a low austenite lattice parameter.

At 925 and 380 °C, i.e. the highest values of the austenitization and austempering temperatures, respectively, the ferrite lattice parameter achieved its largest value, which should be attributed to its highest heterogeneity and the presence of the small fractions of martensite ($<5\%$) in ausferrite both for the thin-walled and reference castings, martensite that was in the blocky austenite areas, as reported in Fig. 1. Such an inhomogeneous structure had a negative effect, having an austenite lattice parameter lower than the value obtained through austempering at 310 °C. So in conclusions it is found that the austenite and ferrite lattice parameters are strictly related to the carbon content and phase fraction in ausferrite, and it can be thus stated that for a given chemical composition the lattice parameters of the constituent phases in ausferrite depend on the austenitization and austempering temperatures, as well as the isothermal annealing time.

The ferrite lattice strain that originated from the static defects in the lattice (e.g., dislocations, vacancies, and disorder) that were generated during phase transformation can be plotted vs. the austenitization and austempering temperatures in Fig. 4.

**Table 1** Chemical composition of ADI castings

| Element | C | Si | Mn | P | S | Ni | Cu | Cr | Mg | Mo | Ce | B |
|---|---|---|---|---|---|---|---|---|---|---|---|---|
| (wt.%) | 3.46 | 2.37 | 0.29 | 0.02 | 0.01 | 1.10 | 0.84 | 0.002 | 0.045 | 0.04 | 0.0026 | 0.002 |
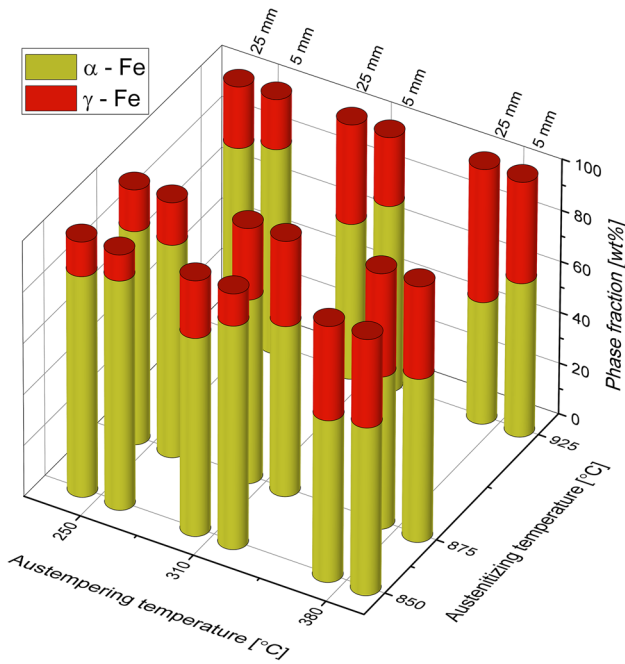


**Fig. 2** Bainitic ferrite and high-carbon austenite weight fractions in ausferrite vs. austenitizing and austempering temperatures in 5 mm walled and reference 25 mm plate castings
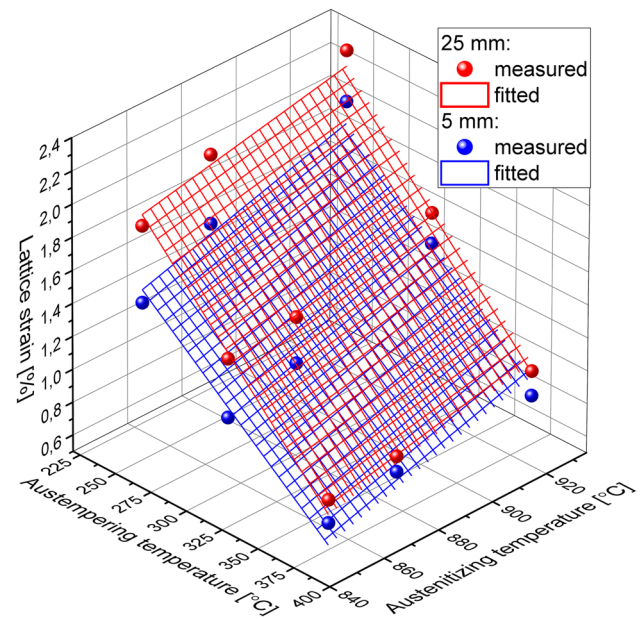


**Fig. 4** Effect on lattice strain of austenitization and austempering temperatures in investigated 5 mm thin-walled and 25 mm walled castings
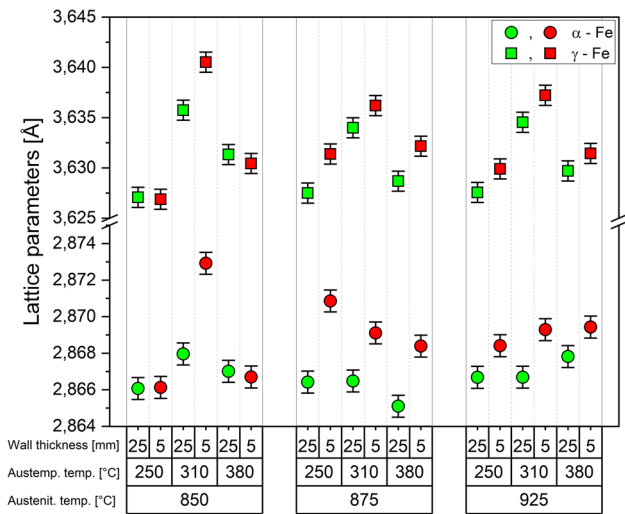


**Fig. 3** Lattice parameters of austenite and ferrite vs. austenitizing and austempering temperatures for 5 mm walled and reference 25 mm walled castings

As is shown in Fig. 4, the lattice strain in the ferrite was linearly related to the austenitizing and austempering temperatures with the highly adjusted $R^2$ being 0.982 and 0.988 for the thin-walled and reference castings, respectively. The refined planes equations are as follows:

$$\sigma_\alpha^{25mm} = -1.2 - 0.0095 \bullet T_{Austemper.} + 0.0037 \bullet T_{Austenit.}[\%], \tag{3a}$$

$$\sigma_\alpha^{5mm} = -1.0 - 0.0074 \bullet T_{Austemper.} + 0.0012 \bullet T_{Austenit.}[\%]. \tag{3b}$$

The utmost lattice strain were observed through austenitizing both thin- and thick-walled castings at 925 °C, and austempering at 250 °C, those are the highest-applied austenitization and the lowest-applied austempering temperatures, respectively. The thin-walled castings showed lower values of lattice strain in the ferrite. This effect was related to the phase contribution in the ADI castings as well as the interaction of the supersaturated carbon contents in the ferrite and austenite. The higher fraction of austenite in the reference castings and also the occurrence of the blocky

austenite where martensite can form generated a significant amount of elastic strain, which led to an increase in the lattice strain. The microstructures of ADI castings (and especially their stability) depend significantly on the carbon content in the austenite and bainitic ferrite. Higher austenitizing temperature affects the austenite carbon content (as reported in [33]), leading to a higher carbon content that in turn makes the ferrite platelets nucleation and growth sluggish. The decrease of driving force for the austempering reaction, in turn, requires longer austempering time for obtaining high-carbon austenite.

## 3.3 Thermal stability

The microstructure stability of ausferrite depends significantly on the carbon content in austenite and bainitic ferrite. Figure 5 shows X-ray diffraction patterns as a function of the changing temperature up to 450 °C for thin and thick-walled ADI samples that were obtained under two different heat treatments.

For temperatures within 25° and 200 °C, no significant variation could be found, whilst above 200 °C the γ-phase reflections deteriorated. For the 850/380 samples, the *111* reflection at $2\theta = 43.1°$ began to diminish above 275 °C and dissolved completely at 420° and 430 °C for the thin-walled and reference castings, respectively. For the other samples (925/380 °C), similar behavior was found. Though the respective temperatures were lower, the γ-phase deterioration began at 220 °C, dissolving at 410 and 430 °C for the thin-walled and reference samples, respectively. It is worth mentioning that the thin-walled specimens exhibited better stability in terms of their structural composition than the reference samples did. The main reflection of the ferrite phase (*110* at $2\theta = 44.6°$) started to gain intensity only when the austenite phase dissolved.

As is apparent in Fig. 5, the positions of the reflections behaved very differently. Namely, the austenite *111* reflection showed a significant shift toward the lower angles for the intermediate temperatures, while it shifted back for the higher ones. This is a sign of phase disproportion.
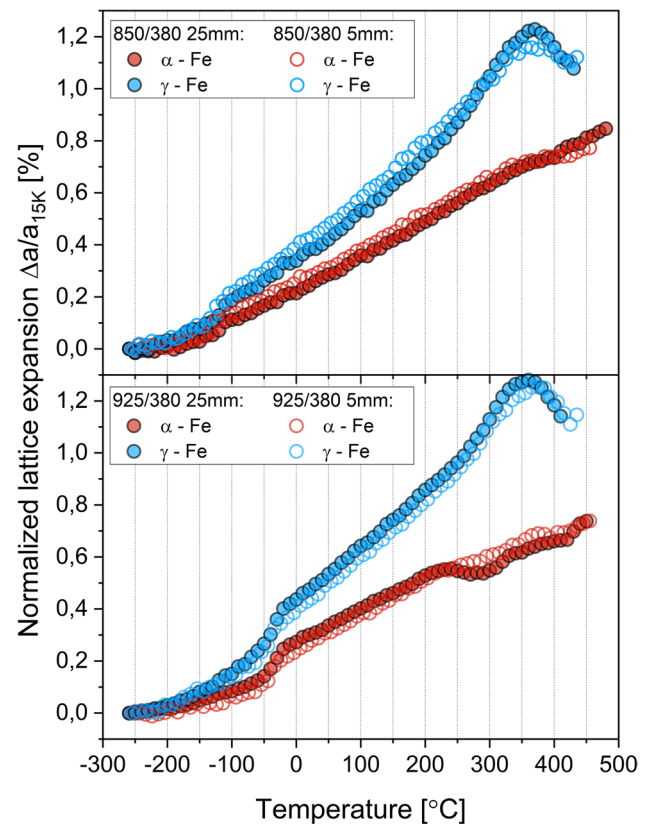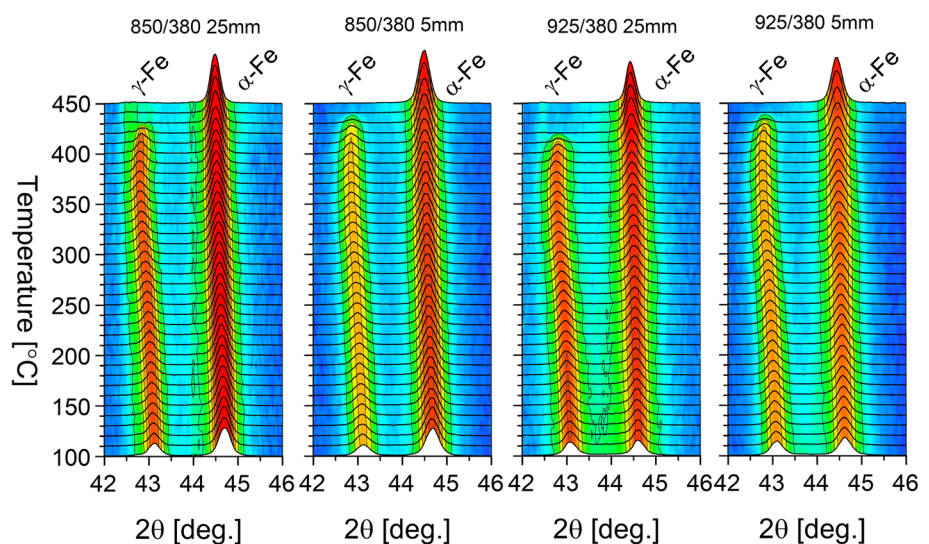


**Fig. 6** Normalized lattice expansion of austenite and ferrite in thin-walled and reference castings vs. different heat-treatment conditions



**Fig. 5** Changing temperature X-ray diffraction patterns vs. temperature of thick and thin-walled ADI produced under two different heat treatments: austenitization at 850 °C and austempering at 380 °C; austenitization at 925 °C and austempering at 380 °C

The Rietveld refinements of the collected diffraction patterns enabled analyses of the thermal stabilities of both the thin and reference castings. The derived normalized lattice expansion as a function of temperature within a range of − 260° to 450 °C for the two extreme austenitizing temperatures, is shown in Fig. 6.

An analysis of the variations in the austenite lattice parameter indicates the significant effect of the austenitizing temperature on the structural stability of the thin and reference castings. For the austenitizing temperature of 925 °C, the thin-walled castings showed greater stability during the heating as compared to the reference castings. It can be observed that, during heating at around 420 °C, the lattice parameter of the ferrite changed significantly due to the reduction of the carbon content in the ferrite that was caused by the precipitation of the independently nucleating cementite $M_3C$. Apparently, the lattice expansion of the martensitic-like phases was twice as high as the ferritic ones, implying significantly different lattice dynamics in the investigated phases. As will be discussed later, this mismatch was the origin of the strain changes with the variation of the temperature.

In the thin-walled castings, the ferrite lattice parameter deviated slightly from its linear growth with temperature, which indicates much lower instability. The lower austenitizing temperature of 850 °C (instead of 925 °C) made the lattice parameters of the ferrite and austenite more stable for the thin-walled castings as compared to the reference castings, also for negative temperatures. This was particularly visible at − 30 °C, where the austenite and ferrite lattice parameters were significantly reduced in the reference castings due to the loss of stability in the high-carbon austenite. Furthermore, the austenite lattice parameters in the thin-walled and reference castings (850/380 °C) were higher than in the ADI that was austenitized at the higher temperature, that is 925 °C. This means that, although in austenite a higher carbon concentration occurred with higher austenitizing temperature before austempering, the resulting austenite carbon content after the austempering process was lower.

The austenite and ferrite share as a function of temperature is shown in Fig. 7, where it can be observed that, upon cooling at − 30 °C, a significant decrease in the fraction of the austenite occurred in the reference castings austenitized at 925 °C, while these changes were much smaller in the thin-section castings. This indicates the thin-walled casting has greater stability. In the reference castings in Fig. 7, a sudden increase occurred in the ferrite fraction during the heating at around 230 °C, since the decrease in the lattice parameter of the ferrite (cementite nucleation) was the result of the martensite tempering in the blocky austenite regions. This effect was slightly visible in the thin-walled castings obtained at the austenitization temperature of 925 °C, and
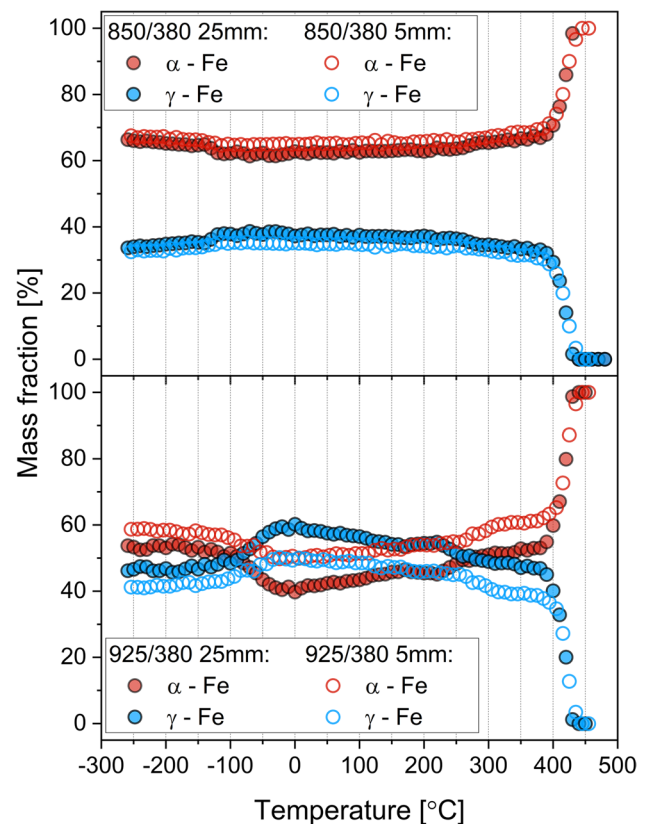


**Fig. 7** Fraction of austenite and ferrite vs. austenitizing and austempering temperatures

not visible in the thin- and 25-mm walled castings that were obtained at the austenitization temperature of 850 °C. In conclusions this was related to the tempering of martensite that was present in the blocky austenite (see Fig. 1).

The variations in the austenite and ferrite lattice parameters with temperature caused lattice strain, as shown in Fig. 8. The lattice parameters of austenite and ferrite increased with rising temperatures in a significantly different way (see Fig. 6): this was related to the different phononic properties. For higher temperatures where thermal atomic diffusion was enabled, the precipitation of the cementite as well as the martensite tempering in the ADI that was austenitized at 925 °C, which involved the release of $Fe_{2.4}C$ carbides into the ADI structure and had the greatest impact in the austenite and ferrite lattice strain (see Fig. 8). This was particularly perceivable in the reference castings at temperatures above 300 °C. With increasing temperature up to 450 °C, a sudden stress reduction in ferrite was found with constantly growing stress in austenite lattice until austenite decomposed into ferrite and cementite. For the thin-walled castings, the lattice strain values were generally lower than in the reference castings through the entire temperature range. From these findings, it can be stated that the lower
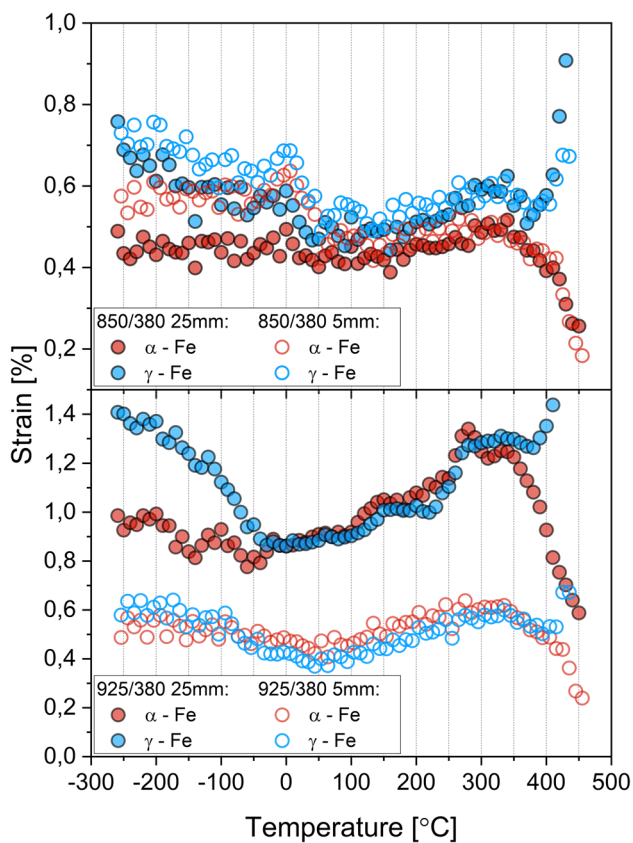
**Fig. 8** Austenite and ferrite strain vs. temperature for 850/380 °C and 925/380 °C samples

austenitization temperature gave the ADI more stability than the higher austenitization temperature.

An analysis of the stability of the ADI castings in the thin-section and reference castings indicates that ADIs can behave unstably during operation at temperatures that are below 0 °C. From the microstructure point of view, the occurrence of unstable blocky austenite is dangerous because, during operation at negative temperature values below − 30 °C, a sudden lattice parameter decrease of austenite and ferrite occurs, as well as a decrease in austenite fraction, and a sudden increase in the austenite lattice stresses occur. This is due to the partial or complete transformation of unstable blocky austenite into martensite. This is because the regular ferrite structure cannot dissolve the carbon content, so the carbon is captured in the tetragonally deformed martensite lattice. The key to high structural stability is to minimize the proportion and size of blocky austenite, which can be achieved by selecting an appropriate austenitizing temperature that significantly affects the kinetics of the austempering transformation. The present research has shown that thin-walled castings obtained at an austenitizing temperature of 850 °C have the highest structural stability among the investigated conditions, which is

manifested in first approximation by the linear changes of the austenite and ferrite lattice parameters that are characteristic for the absence of phase transitions in the solid state. The lower austenitizing temperatures guarantee the higher driving forces for the solid-state austempering transformation, reducing the presence of blocky austenite that did not contribute to austempering because of low driving force [7]. On the other side, the higher homogeneity of chemical composition and microstructure with shorter interparticle spacing typical of thin-wall castings which affect the kinetics of austempering [7, 22], produced the more stable ausferrite with a higher number of ferrite plates packets.

According to the authors, the above analysis may convince designers of high-tech components to use high-quality thin-walled ADI castings that are characterized by good mechanical and functional properties whose production cost is relatively low. From the point of view of economy and ecology, thin-walled castings that are made of ductile iron (especially ADI) can compete in terms of mechanical properties with light castings that are made of aluminum alloys from the group of high-strength Al-Cu and Al-Si alloys that are subjected to T6 heat treatment.

## 4 Conclusions

In this work, we analyzed the effects of casting thickness and heat-treatment-process parameters on the structural and thermal stability of ADIs. X-ray diffraction (XRD) investigations with changing temperature were performed between − 260 up to + 450 °C to investigate the change of phase fraction, lattice parameters and strain in ausferrite. The following conclusions can be drawn:

1. The detrimental occurrence of "blocky" high-carbon austenite that could not be completely transformed during austempering, was noticeable both in the thin-walled sections and in the reference castings, but at the highest austenitizing and austempering temperatures, that is, 925° and 380 °C, respectively, the conditions for which the driving force for austempering solid-state transformation is lower.

2. The 5 mm thin-walled ausferritic castings provided a more stable structure than the 25 mm castings over a wide temperature range, from − 260 °C up to 450 °C. In the thin-walled castings that had a short interparticle distance, the austenite grain size was much smaller as compared to that which was formed in the castings with the larger wall thicknesses and lower cooling rates. This resulted in a higher microstructure homogeneity with a greater number of ferrite plate packets, which resulted to be beneficial to the stability of ausferrite.

3. The key to high structural stability is to minimize the proportion and size of the blocky austenite, which can be achieved by selecting an appropriate austenitizing temperature that significantly affects the kinetics of the austempering transformation.

**Data availability** The data that support the findings of this study are available from the corresponding author, [MG], upon reasonable request.

## Declarations

**Conflict of interest** All authors certify that they have no affiliations with or involvement in any organization or entity with any financial interest or non-financial interest in the subject matter or materials discussed in this manuscript.

## References

1. Bamberger M. Encyclopedia of iron, steel and their alloy. 5th ed. New York: Taylor and Francis; 2016. p. 196–216.
2. Holtzer M, Górny M, Kmita A. The influence of motorisation on the climate warming. Int J Global Warm. 2017;11:495–514.
3. Myszka D, Cybula L, Wieczorek A. Influence of heat treatment conditions on microstructure and mechanical properties of austempered ductile iron after dynamic deformation test. Arch Metall Mater. 2014;59:1181–9.
4. Chernyshev AN, Kaplina IN, Serapin MI. Surface hardening with remelting of functional surfaces of cast iron camshafts. Met Sci Heat Treat. 1996;38:440–2.
5. Tanaka Y, Kage H. Development and application of austempered spheroidal graphite cast iron. Mater Trans JIM. 1992;33:543–57.
6. Górny M, Stefanescu DM. ASM Handbook. Cast iron science and technology. ASM International; 2017. pp. 626–628.
7. Górny M, Gondek Ł, Tyrała E, Angella G, Kawalec M. Structure homogeneity and thermal stability of austempered ductile iron. Metall Mater Trans A. 2021;52:2228–37
8. Rouns TN, Rundman KB, Moore DM. On the structure and properties of austempered ductile cast iron. AFS Trans. 1984;121:815–40
9. Dubensky W, Rundman KB. An electron microscope study of carbide formation on austempered ductile iron. AFS Trans. 1985;93:389–94.
10. Donnini R, Fabrizi A, Bonollo F, Zanardi F, Angella G. Assessment of the microstructure evolution of an austempered ductile iron during austempering process through strain hardening analysis. Met Mater Int. 2017;23:855–64.
11. Fraś E, Górny M, Tyrała E, Lopez HF. Effect of nodule count on austenitising and austempering kinetics of ductile iron castings and mechanical properties of thin walled iron castings. Mater Sci Tech. 2012;28:1391–6.
12. Górny M, Tyrała E, Lopez H. Effect of copper and nickel on the transformation kinetics of austempered ductile iron. J Mater Eng Perform. 2014;23:3505–10.
13. Ahmed M, Soliman M, Youssef M, Bahr R, Nofal A. Effect of niobium on the microstructure and mechanical properties of alloyed ductile irons and austempered ductile irons. Metals. 2021;11:703.
14. Gazda A. Analysis of decomposition processes of ausferrite in copper–nickel austempered ductile iron. J Therm Anal Calorim. 2010;102:923–30.
15. Hegde A, Sharma S, Vikas SR. Mechanical characterization and optimization of heat treatment parameters of manganese alloyed austempered ductile iron. J Mech Eng Sci. 2019;13(1):4356–67.
16. Colin-García E, Cruz-Ramírez A, Romero-Serrano JA. Nodule count effect on microstructure and mechanical properties of hypo-eutectic ADI alloyed with nickel. J Min Metall Sect B Metall. 2021;57:115–24.
17. Bakhshinezhad H, Honarbakhshraouf A, Abdollah-Pour H. A study of effect of vanadium on microstructure and mechanical properties of as-cast and austempered ductile iron. Phys Met Metallogr. 2019;120:441–6.
18. Haydarzadeh SM, Nili AA, Bahrami VA. The role of austempering parameters on the structure and mechanical properties of heavy section ADI. J Mater Process Technol. 2004;153:203–8
19. Zhang H, Wu Y, Li Q, Hong X. Mechanical properties and rolling-sliding wear performance of dual phase austempered ductile iron as potential metro wheel material. Wear. 2018;406–407:156–65.
20. Kim YJ, Shin H, Park H. Investigation into mechanical properties of austempered ductile cast iron (ADI) in accordance with austempering temperature. Mat Lett. 2008;62(3):357–60.
21. Hegde A, Sharma S, Shankar MC. Machinability and related properties of austempered ductile iron: a review. J Mech Eng Sci. 2018;12(4):4180–90.
22. Górny M, Angella G, Tyrała E, Kawalec M, Paź S, Kmita A. Role of austenitization temperature on structure homogeneity and transformation kinetics in austempered ductile iron. Met Mat Int. 2019;25(4):956–65.
23. Taran YN, Uzlov KI, Kutsov AY. The bainite reaction kinetics in austempered ductile iron. J de Phys IV. 1997;7(5):429–34.
24. Boccardo A, Dardati M, Celentano DJ, Godoy LA, Gorny M, Tyrała E. Numerical simulation of austempering heat treatment of a ductile cast Iron. Metall Trans B. 2016;47:566–75.
25. Boccardoa AD, Dardatib PM, Godoya LA, Celentanod DJ. Sensitivity of austempering heat treatment of ductile irons to changes in process parameters. Metall Trans B. 2018;49:1522–36.
26. Massone J, Boeri R, Sikora J. Changes in the structure and properties of ADI on exposure to high temperatures. Int J Cast Metal Res. 1996;9:79–82.
27. Pérez MJ, Cisneros MM, Valdés E. Experimental study of the thermal stability of austempered ductile irons. J Mater Eng Perform. 2002;11:519–26.
28. Li X, Soria S, Gan W. Multi-scale phase analyses of strain-induced martensite in austempered ductile iron (ADI) using neutron diffraction and transmission techniques. J Mater Sci. 2021;56:5296–306.
29. Rodriguez-Carvajal J. Recent advances in magnetic structure determination by neutron powder diffraction. Physica B. 1993;192:55–69.
30. Dantzig AJ, Rappaz M. Solidification. EPFL Press, 2016.

31. Górny M, Tyrała E, Sikora G, Rogal Ł. Identification of Mg$_2$Cu particles in Cu-alloyed austempered ductile iron. Met Mater Int. 2018;24:95–100.

32. Takahashi T, Abe T, Tada S. Effect of bainite transformation and retained austenite on mechanical properties of austempered spheroidal graphite cast steel. Metall Mater Trans A. 1996;27A:1589–98.

33. Darwish N, Elliott R. Austempering of low manganese ductile irons. Mater Sci Technol. 1993;9:572–85.